POLY(2-N-PROPYL-2-OXAZOLINE)/TANNIC ACID NANOCAPSULES WITH *IN-SITU* SYNTHESIZED GOLD NANORODS FOR CANCER THERANOSTICS

Varsha Sharma[1], Maarten Vergaelen[2], Sangamithra Nehru[3], Richard Hoogenboom[2]*, Anandhakumar Sundaramurthy[4]*

[1]Department of Biomedical Engineering, College of Engineering and Technology, SRM Institute of Science and Technology, Kattankulathur- 603203, Chengalpattu, Tamil Nadu, India.

[2]Supramolecular Chemistry Group, Centre of Macromolecular Chemistry (CMaC), Department of Organic and Macromolecular Chemistry, Ghent University, Krijgslaan 281 S4, B-9000, Ghent, Belgium.

[3]Department of Physics and Nanotechnology, College of Engineering and Technology, SRM Institute of Science and Technology, Kattankulathur- 603203, Chengalpattu, Tamil Nadu, India.

[4]Department of Chemical Engineering, College of Engineering and Technology, SRM Institute of Science and Technology, Kattankulathur- 603203, Chengalpattu, Tamil Nadu, India.

Corresponding Authors*:

Dr. Anandhakumar Sundaramurthy
Associate Professor, Biomaterial Research Laboratory
Department of Chemical Engineering
SRM Institute of Science and Technology, Chengalpattu-603203, India.
Email: anandhas@srmist.edu.in**;** rsanandhakumar@gmail.com

Prof. Richard Hoogenboom
Supramolecular Chemistry Group, Centre of Macromolecular Chemistry (CMaC)
Department of Organic and Macromolecular Chemistry
Ghent University, Krijgslaan 281 S4, B-9000, Ghent, Belgium

Email: Richard.Hoogenboom@ugent.be

ABSTRACT

The concept of hollow polymeric capsules fabricated with thermoresponsive polymers has revealed immense possibilities in the field of nanomedicine due to their tunable temperature and pH responsiveness caused by lower critical solution temperature (LCST) behavior. Herein, we report a new methodology to *in-situ* synthesize gold nanorods (AuNRs) within the pores of mesoporous silica nanoparticles (NPs) by trapping gold seed crystals and growing them into NRs in the presence of a weak reducing agent. The mesoporous silica NPs with incorporated NRs, i.e., modified silica NPs (SiO_2-NRs) were used as sacrificial template for the fabrication of hollow polymeric multilayer capsules *via* layer-by-layer (LbL) assembly using poly(2-*n*-propyl-2-oxazoline) (P*n*PrOx) and tannic acid (TA) as layer components. The NRs of 25 ± 5 nm in size were uniformly distributed in the interior structure of P*n*PrOx/TA nanocapsules. The photo-thermal conversion efficiency of the P*n*PrOx/TA nanocapsules was found to be 47.5%. The release of encapsulated doxorubicin was found to be 55%, which increased to 68% when the incubation time was increased from 1 to 2 h. An on-demand burst release of 56% of the drug occurred within 2 min of NIR light exposure, and it reached 72% within 30 min, which inflicted major damage to cancer cells. Notably, the capsule suspension temperature increase from room temperature to 47 ºC under laser light exposure, which is not only playing a key role in rupturing the capsules to enhance the drug release but also induces a hyperthermia effect in the tumor environment. Further, the *in-vitro* cytotoxicity experiments with human epithelial HEp-2 cells and fibrosarcoma HT1080 cells revealed an enhanced anti-cancer activity due to a synergistic chemo-photothermal effect. Hence, the proposed nanocapsule system can provide a unique, cheap, and efficient way of fabricating cancer theranostics for *in-vivo* applications.

Keywords: Temperature responsive nanocapsules, Tannic acid, Poly(2-*n*-propyl-2-oxazoline), Gold nanorods, *in-situ* synthesis, On-demand release.

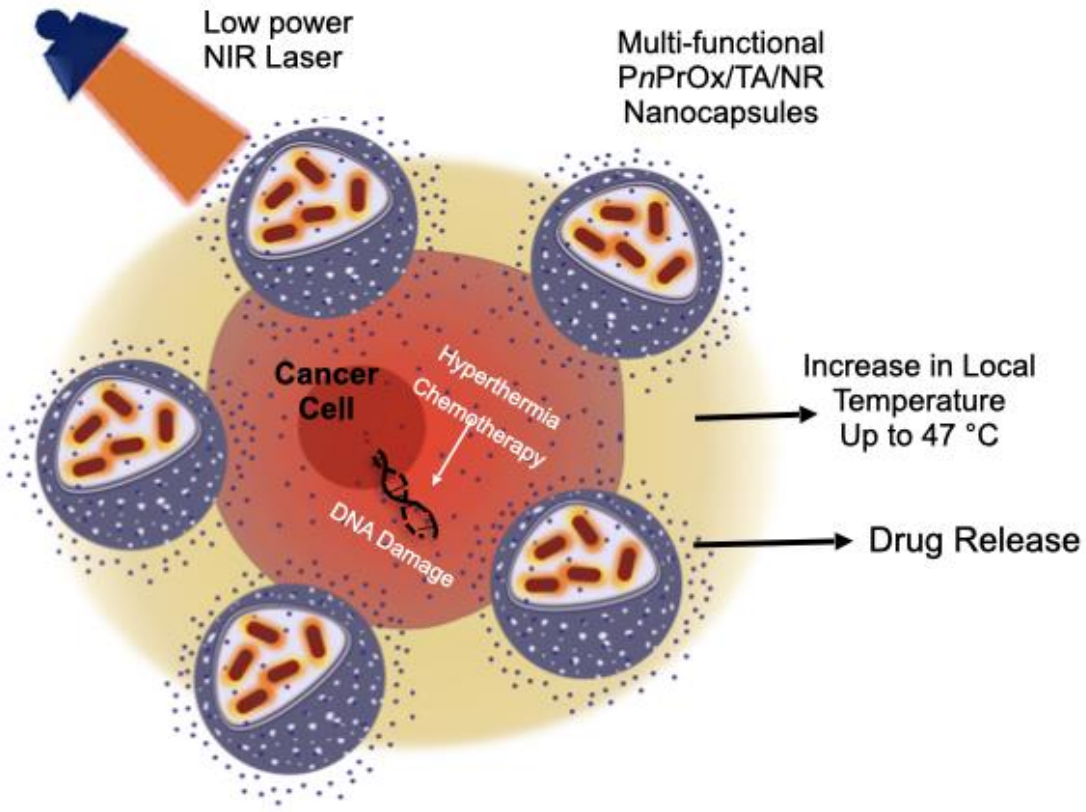

Abstract Image. Schematic representation of effective *in vitro* cancer treatment by NIR-irradiation of P*n*PrOx/TA/NR nanocapsules.

1. INTRODUCTION

In recent years, poly(2-alkyl-2-oxazoline) (PAOx) based systems are being explored exhaustively, as they are structurally similar to peptides and have interesting properties for biological applications, such as biocompatibility, long-term chemical stability, anti-fouling, stealth behavior and easy renal clearance [**1-4**]. The interaction of PAOx with naturally occurring polyphenols (e.g., tannic acid (TA)) *via* hydrogen bonding is highly beneficial for providing better stability for the formed capsules at physiological conditions, while also inducing pH and temperature responsiveness [5]. Among the various PAOx systems, poly(2-*n*-propyl-2-oxazoline) (P*n*PrOx) is an interesting stimuli-responsive polymer as it has a cloud point temperature (T_{CP}) of ~25 °C. As a result, it can easily undergo a configurational transformation from extended hydrated form to a collapsed globular form at a physiological temperature of 37 °C, which results in pore formation followed by rupture of capsules as a function of time. Our previous investigations revealed that the combination of hydrophobic interactions and hydrogen bonding play an important role in stabilizing the P*n*PrOx/TA films and make them stable over a wide pH range from 2 to 9 [**5**]. The follow-up studies on P*n*PrOx/TA capsules showed the permeability of multilayer shell switching from closed to open state by undergoing configurational reorganization and formation of aggregates in the capsule shell at elevated temperatures [6]. Moreover, P*n*PrOx/TA/gellan gum (GG) macro-sized capsules pre-loaded with emulsions were recently fabricated using P*n*PrOx above T_{CP}, for the oral delivery of model hydrophobic (vitamin) supplements and lipase enzyme [**6**]. Thereby P*n*PrOx is acting as a Pickering emulsion at the GG interphase in the initial stage of capsule formation and subsequently forms hydrogen bonds with TA in the second step resulting in enhanced stability for the formed P*n*PrOx/TA/GG capsules. Notably, the fabricated capsules were able to protect the encapsulated enzymes from harsh simulated gastric fluid environment and successfully delivered them in simulated intestinal conditions. Previous investigations on P*n*PrOx also demonstrate that thermoresponsive behavior also played an important role in cell harvesting processes [7]. When P*n*PrOx was immobilized on glass wafers through a poly(glycidyl methacrylate) anchor layer in chloroform and later subjected to annealing at 150 °C under vacuum for 16 h, the surface grown L929 and Vero cells were easily detached from P*n*PrOx surface by simply lowering the temperature of the system to 8 °C [**7**]. Hence, P*n*PrOx based systems are continuously explored for various biomedical applications ranging from antibacterial coatings, cell harvesting process and drug and enzyme delivery to catalysis [2-4,6-8].

Several reports describe the formation of multilayer capsules incorporated with anisotropic NPs, especially gold nanorods (NRs), as they can be potential candidates for absorbing near-infrared (NIR) light and generating heat for photothermal therapy (PTT) without any issue concerning deep tissue penetration. The anisotropic NPs are commonly synthesized by the seed mediated method and the preformed anisotropic NPs such as bipyramids and NRs have been easily incorporated during the synthesis of the sacrificial micro template, which is later used for the fabrication of microcapsules [**9**-**10**]. Further, the direct growth of NRs on the surface of preformed poly(allylamine hydrochloride)/poly(styrene sulfonate) capsules have also been reported by the seed mediated method [**11**]. Even though this method provided good encapsulation of NRs, there is a high possibility for the detachment of anisotropic NPs from the capsule surface after a few washes. To circumvent this limitation, a sequential deposition of NRs and silica NPs was demonstrated on polystyrene beads *via* electrostatic interactions [**12**]. Furthermore, core-shell hybrid structures were synthesized using NRs with poly(o-methoxyaniline) (POMA) through a surfactant-assisted chemical oxidative polymerization for photothermal therapy [**13**]. Notably, the temperature increment and photo-thermal conversion efficiency (PCE) were estimated to be 20 °C and 18.7% under exposure of NIR light of 808 nm and 3 W, respectively. It is generally believed that the low photo-thermal heat generation and PCE significantly affect the performance of capsules in chemo-photothermal therapy. Though many anisotropic NPs were reported for high PCE, their incorporation into hollow capsules drastically reduced the heat generation, which in turn, limited their potential in cancer therapy. For instance, the PCE of NRs was estimated to be 22.3% and it decreased to ~18% after their incorporation into NRs/POMA core/shell structures [**13**]. Hence, alternative methodologies are being explored to improve the encapsulation of anisotropic NPs and enhance the photo-thermal heat generation. In one such attempt, hard and rough rattle shaped Au@hollow silica NPs-poly(glycidyl methacrylate) core-shell NPs have been reported for chemo-PTT [**14**]. The *in-situ* synthesized NRs in the interior of nanostructures resulted in a temperature increase of 20 °C at a concentration of 200 $\mu g.mL^{-1}$ which increased to 46 °C when the concentration of NRs was increased to 800 $\mu g.mL^{-1}$ at 2 $W.cm^{-2}$ and 808 nm [**14**]. Inspried by those reported studies, we believe that *in-situ* synthesis of NRs inside hollow P*n*PrOx/TA nanocapsules through a new methodology might open-up a new avenues for cancer therapy. Moreover, new attempts are required to improve the PCE, photo-thermal heat generation and ability to release loaded molecules in an on-demand manner, which is not only resulting in higher local temperature, i.e., hyperthermia, but also maintains high drug concentration (chemotherapy) in the tumor environment. Hence, any possibility of

imparting temperature and pH responsiveness in the resulting multilayer capsules will be highly advantageous as the release of loaded drugs can be controlled in a specific manner, i.e., sustained or burst release. Amongst these, the release of the entire payload in one go will allow us to increase the local drug concentration beyond IC_{50} value of cancer cells to inflict major damage to cancer cells. Herein, we have fabricated P*n*PrOx/TA nanocapsules containing NRs via a novel *in-situ* synthesis methodology for on-demand laser light activated delivery of DOX for cancer chemo-photothermal therapy. We successfully report the preparation of the PAOx/TA based nanocapsules and demonstrate the *in-situ* synthesis of NRs in the pores of mesoporous silica NPs via modified layer-by-layer (LbL) assembly. These capsules have the ability to release the encapsulated molecules in a burst manner within few minutes or in a controlled manner for few hours. To the best of our knowledge, the *in-situ* synthesis of NRs into the pores of silica NPs and their incorporation into hollow nanocapsules has not yet been explored for cancer therapy. Hence, in this study, we demonstrate improvement of PCE and heat generation on the one hand while providing temperature and pH responsiveness, using PAOx, for the resulting capsules on the other hand.

In this work, the *in-situ* synthesis of gold NRs have been demonstrated within the P*n*PrOx/TA hydrogen bonded nanocapsules, providing temperature responsiveness and on-demand triggered release of the payload using NIR irradiation, for the application in cancer chemo-photothermal therapy. The NRs were grown *in-situ* within the mesoporous silica template, to obtain a higher number of NRs encapsulation. The applicability of the method was successfully utilized for TA/poly(2-ethyl-2-oxazoline) (PEtOx) and TA/poly(2-methyl-2-oxazoline) (PMeOx) nanocapsules. Subsequently, the fabricated capsules were characterized by scanning electron microscopy (SEM), UV-Visible spectroscopy, and transmission electron microscopy (TEM). Next, as proof-of-concept, a model anticancer drug, doxorubicin hydrochloride (DOX), was loaded into the capsules and its release profile was studied at 37 °C and under NIR exposure. Finally, the *in-vitro* cytotoxicity of the system was studied with HEp-2 human epithelial cells and HT1080 fibrosarcoma cells as a function of time under fluorescent staining.

2. EXPERIMENTAL SECTION

2.1 Chemicals

Tannic Acid (TA), mesoporous silica particles (SiO_2, pore size ~4 nm), hydrofluoric acid (HF), ammonium fluoride (NH_4F), auric chloride ($HAuCl_4$),

cetyltrimethylammonium bromide (CTAB), ascorbic acid (AA), doxorubicin (DOX), propidium iodide (PI), acridine orange (AO), ethidium bromide (EtBr), Dulbecco's modified eagle medium (DMEM), fetal bovine serum (FBS), gentamicin and AlamarBlue™ were purchased from Sigma-Aldrich. Sodium borohydride ($NaBH_4$), silver nitrate ($AgNO_3$), trisodium citrate and phosphate buffered saline (PBS) were purchased from SRL India Pvt. Ltd. P*n*PrOx, PEtOx and PMeOx were synthesized by microwave-assisted cationic ring-opening polymerization (CROP), as reported earlier (**Supporting Information, Table T1**) [**15**]. The chemicals were of analytical grade and used as received. All the experiments were performed with freshly prepared stock solutions. Milli-Q water with a resistivity of >18.2 MΩ.cm at 25˚C from the Millipore water purification system, was used for all experiments.

2.2 Synthesis of modified SiO_2 nanotemplates

Mesoporous SiO_2 NPs (~50 mg) were washed three times with water and used for the *in-situ* growth of gold NRs. The Au seeds were prepared from 5 mL of $HAuCl_4$ (0.5 mM), 5 mL of CTAB (0.2 M) and 0.6 mL of ice-cold $NaBH_4$ (0.01 M) as reported in our previous studies [**9-10**]. The obtained brown colored seed suspension was kept for 10 min at 25 °C, whereafter the washed SiO_2 particles were introduced in the suspension, followed by a further incubation time of 30 min. During this course of time, the Au seeds (2-4 nm) penetrated the pores of the nanotemplate (~4 nm). Thereafter, 2 mL of TA solution (1 $mg.mL^{-1}$) was added into the seed solution and incubated for another 15 min to form a layer surrounding the template to trap the embedded seed particles into the pores of SiO_2. Next, this seed solution was centrifuged at 8000 rpm for 10 min and washed once with DI water. Further, the obtained SiO_2 NPs with entrapped seeds were added in the growth solution (5 mL of 1 mM $HAuCl_4$, 0.2 mL of 4 mM $AgNO_3$, 5 mL of 0.2 M CTAB and 0.07 mL of 78.8 mM AA) to grow NRs inside the silica NPs. The growth solution was left undisturbed for 30 min at room temperature (RT, 27 °C). After completion of NR formation, the SiO_2 NPs with *in-situ* synthesized NRs (SiO_2-NRs) were washed several times using milli-Q water and stored before further use.

2.3 Fabrication of control and modified multilayer hollow nanocapsules

The hollow multilayer capsules were prepared by LbL deposition method as reported earlier [**16-17**]. The P*n*PrOx and TA stock solutions (0.5 $mg.mL^{-1}$) were prepared in water and used for LBL assembly. Prior to multi-layer film formation, the SiO_2-NR nanotemplate was washed two times with water through centrifugation process in 2 mL centrifuge tubes (Hermle Labortechnik, Germany). To coat the first layer, 2 mL of the first

polymer solution was added to the tube and incubated for 15 min, followed by thorough washing with water for three times. It should be noted that the first layer of TA was already coated during the *in-situ* preparation of NRs in the template, thus, the LbL assembly was started with P*n*PrOx polymer and alternate deposition of the two materials was continued up to a total of 8 layers, forming $(PnPrOx/TA)_4$ shell. The excess of unbound molecules was removed at every step by thorough washing with milli-Q water. Finally, the SiO_2 template was dissolved by incubating them in HF buffer (0.1 M HF with 0.5 M NH_4F), thereby, leaving free NRs trapped inside the hollow polymeric shell. To estimate the yield of AuNRs in nanocapsules, 1 mL of capsule suspension was dried overnight at 50 °C and weighed in an electronic balance. Later, the capsules were burnt in a furnace at 500 °C, cooled to room temperature and weighed again to estimate the amount of AuNRs present in the capsule suspension.

For the formation of control capsules, the SiO_2 nanotemplates were used as obtained. For the LbL assembly process, the temperature was maintained below the T_{CP} ~25 °C of P*n*PrOx to fabricate the assembled films in hydrated configurational arrangements.

2.4 Drug encapsulation

The encapsulation of hydrophilic therapeutic drug (DOX) was investigated by UV-Visible spectroscopy. The multilayer capsules were dispersed in 2 $mg.mL^{-1}$ of drug solution for 1.5 h and washed one time with water via centrifugation process. The quantification of encapsulated DOX was done by analyzing the difference in supernatant absorbance at 485 nm before and after the encapsulation process [**18-19**]. The drug present in the washing water was estimated at 485 nm and considered as loss, which was later deducted from the amount of encapsulation. The encapsulation efficiency (EE) was calculated by the following equation:

$$EE\% = \frac{\text{Amount of drug loaded in the capsules}}{\text{Initial amount of drug}} \text{ x } 100 \quad (1)$$

2.5 *In-vitro* drug release

A single batch of high volume of drug-loaded capsules was prepared and used for the drug release experiments to get consistent results. The drug release was performed in PBS at pH 7.4, in an incubator shaker at 37 °C and 100 rpm. The drug-loaded capsules were equally divided into a series of micro-centrifuge tubes, depending on the number of time points. One of the tubes was centrifuged at a specific time interval and the obtained supernatant was used to estimate the amount of drug release at that time point, using a UV-Visible spectrophotometer

at 485 nm. The amount of drug released directly corresponds to the absorbance of the supernatant [**18**]. The supernatant of each tube was periodically replaced to maintain the concentration gradient and induce the drug release process. The drug release was also estimated in the presence of NIR light to get more information about the release process under NIR light exposure at 37 °C.

Separately, the release experiments were also conducted at 16 °C (i.e, $T < T_{CP}$).

2.6 Photo-thermal heat generation

A solid-state focusable continuous-wave laser set-up was used to investigate the rupturing capability of the capsules and the release of DOX (808 nm, 0.5 $W.cm^{-2}$, Hitsan, India). The sample suspension (100 μL) was placed in a 1.5 mL microcentrifuge tube and placed directly underneath a mounted laser setup (**Supporting Information, Figure S1**). The temperature was monitored using a probe thermometer and a thermal camera (FLIR Systems, United States). The PCE of the capsules was determined by:

$$\eta = \frac{m\, c_p (T_2 - T_1)}{I(1 - 10^{-Abs_{808}})} \quad (2)$$

Where, m is the mass of water, η is the efficiency, c_p is the specific heat capacity of water, T_1 is the initial temperature, T_2 is the maximum temperature, Abs_{808} is the absorbance of the capsules at 808 nm and I is the laser power. The capsules without NRs and only water was used as control samples and all the experiments were performed in triplicates.

2.7 Anti-cancer activity investigations

The HEp-2 human epithelial cells were grown in 200 μL of DMEM containing 10% FBS and 1% gentamicin solution in an environment maintained at 5% carbon dioxide and 37 °C. Prior to anticancer investigations, the medium was replaced with a low serum medium (1%) and incubated for 4 h. AlamarBlue™ assay was used to determine the cell viability by detecting the metabolically active cells and analyzing the cell viability quantitatively. AlamarBlue™ contains resazurin compound which is a cell-permeable compound and is converted to resorufin after entering the cells. The generated resorufin is red in colour, highly fluorescent and helpful in identifying the dead cells. The cells were treated with different samples for 24 h followed by the addition of AlamarBlue™ for 4 h. The cell viability was then detected by measuring the absorbance of the wells. The absorbance of the wells was measured at 570 and 600 nm, and the cell viability was calculated by the following equation,

$$\text{Cell Viability} = \frac{\text{Sample } [(Abs_{570} * 117216) - (Abs_{600} * 80586)]}{\text{Control } [(Abs_{570} * 117216) - (Abs_{600} * 80586)]} \text{ X } 100 \quad (3)$$

Where, Abs_{570} is the absorbance of sample/control at 570 nm and Abs_{600} is the absorbance of sample/control at 600 nm. The results were compared to a set of control samples including only cells and NIR exposed cells. Additionally, another set of cells was treated with similar samples followed by staining with AO and PI. AO being cell permeable stains both live and dead cells and generates green fluorescence, whereas PI is impermeable to cells and stains only dead cells in a population. Thereafter, the fluorescent images and object count in each image was analyzed via CytoSMART Lux3 fluorescence microscope.

3. RESULTS AND DISCUSSION

3.1 *In-situ* synthesis of NRs and fabrication of P*n*PrOx/TA/NR nanocapsules

The silica nanotemplate (350 ± 50 nm) was modified with NRs *via in-situ* synthesis of the gold NRs by a modified-seed mediated method, as shown in **Scheme 1**. Herein, we attempted to synthesize NRs in the pores of mesophorous silica NPs by physically trapping gold nanoseeds in the porous network of silica NPs followed by its growth into NRs using AA in the presence of shape directing agent, CTAB. While the strong reducing agent ($NaBH_4$) was used for seed crystal formation, the weak reducing agent, AA was used for growing Au seeds into NRs in the interior pores of mesoporous silica NPs. Initially, the gold seeds of ~4 nm were formed by the reduction of gold ions in the presence of CTAB and $NaBH_4$ as shape-directive and strong reducing agents, respectively. After seed crystal formation, the suspension was added with mesoporous SiO_2 NPs to allow seed crystals to move into the pores of the silica nanotemplate (**Figure 1b)**. Even though seeds were not clearly visible in the core, the successful penetration and trapping of Au seeds was confirmed by TEM (**Figure 1c**), wherein the seeds are marked in red circles to stress their presence. Additionally, it was also confirmed by energy dispersive X-ray (EDS) analysis and the resulting elemental composition of silica template is given in **Supporting Information, Figure S2 and Table T2.** Prior to NR formation, the seed embedded SiO_2 particles were coated with a layer of TA to ensure the entrapment of the seeds in the pores. Later, the seed crystals were grown into NRs by adding growth solution containing CTAB and AA. In a next step, the hollow P*n*PrOx/TA/NR nanocapsules were fabricated by LbL deposition of P*n*PrOx and TA on the modified silica

template followed by core dissolution with HF as reported in our previous reports [**20,21**]. The resulting nanocapsules were found to be ~400 nm in size with a shell thickness of ~50 nm. Notably, the NRs of 25 ± 5 nm in size were found to be distributed uniformly in the interior of the capsules confirming successful encapsulation of NRs (**Figure 2**). Interestingly, there was no notable change in size and morphology of nanocapsules containing NRs and control capsules (without NRs). Though previous investigations demonstrated that the template dissolution with HF buffer did not affect the capsule morphology [**20-22**], a separate experiment was performed by treating the preformed NRs in HF buffer and their morphological changes were investigated by HR-TEM. It was found that there was hardly any change in the size and morphology of the NRs (**Supporting Information, Figure S3**). It is noteworthy that the proposed method resulted in uniform formation of NRs inside the hollow capsules in high yield, i.e., 0.2 mg of NRs in 0.4 mg of dry P*n*PrOx/TA/NR capsules. The attempts to fabricate silica templates containing NRs by adding preformed NRs during silica NPs synthesis was not successful as the NRs were mostly observed in the supernatant (**Supporting Information, Figure S4**) [**23**]. The results obtained without the polymeric entities but showing high encapsulation of NRs (**Figure 2c**), with the *in-situ* synthesis method described above, imply high potential in fabricating hollow polymeric capsules encapsulated with various shaped nanomaterials for wide range of applications.

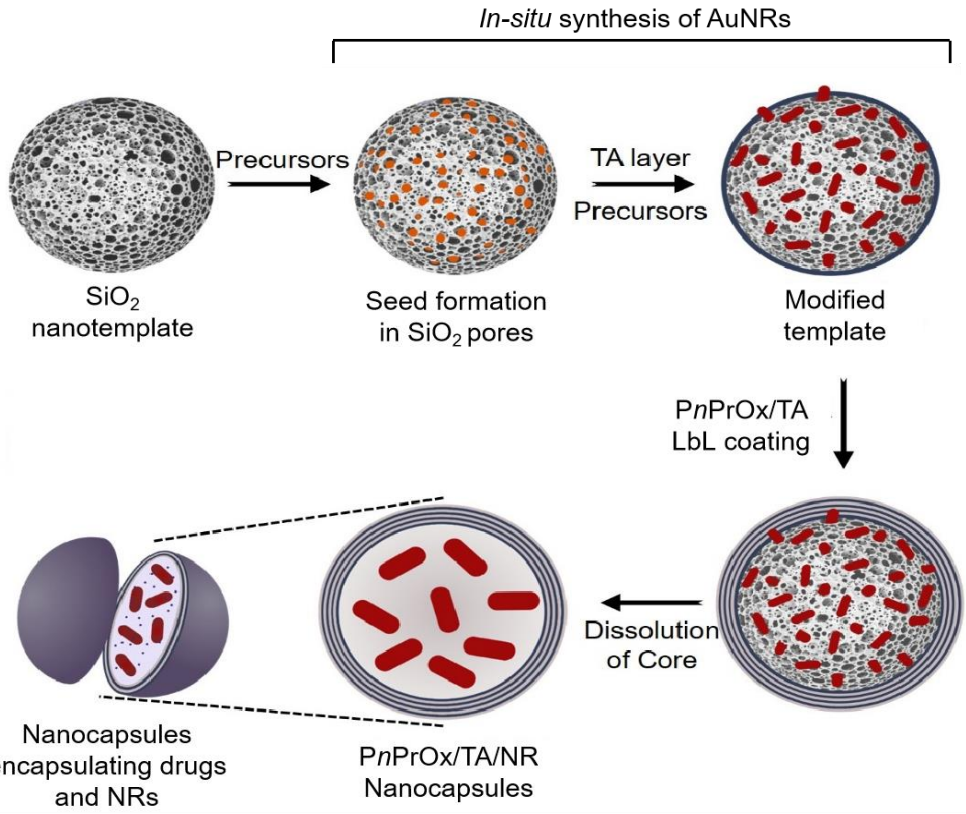

Scheme 1. Schematic illustration showing the fabrication of P*n*PrOx/TA/NR nanocapsules.

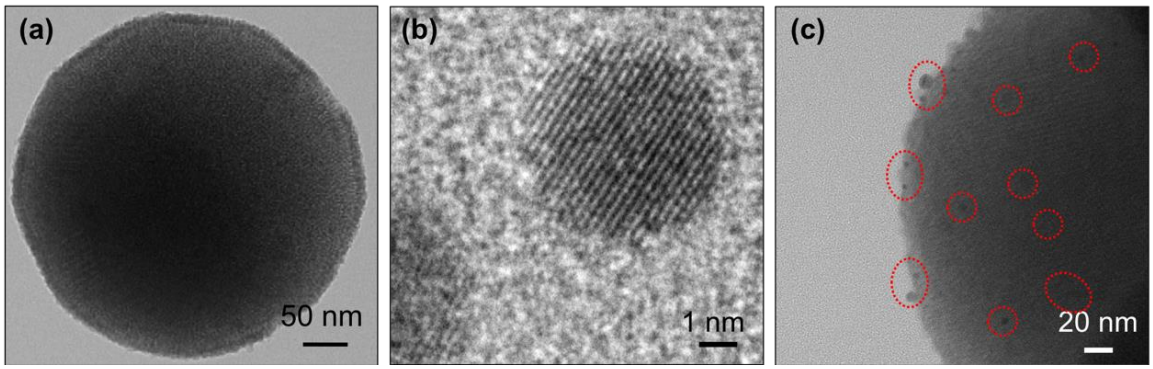

Figure 1. TEM investigation of (a) SiO_2 particle, (b) Au seed crystal and (c) SiO_2 particle embedded with Au seeds.

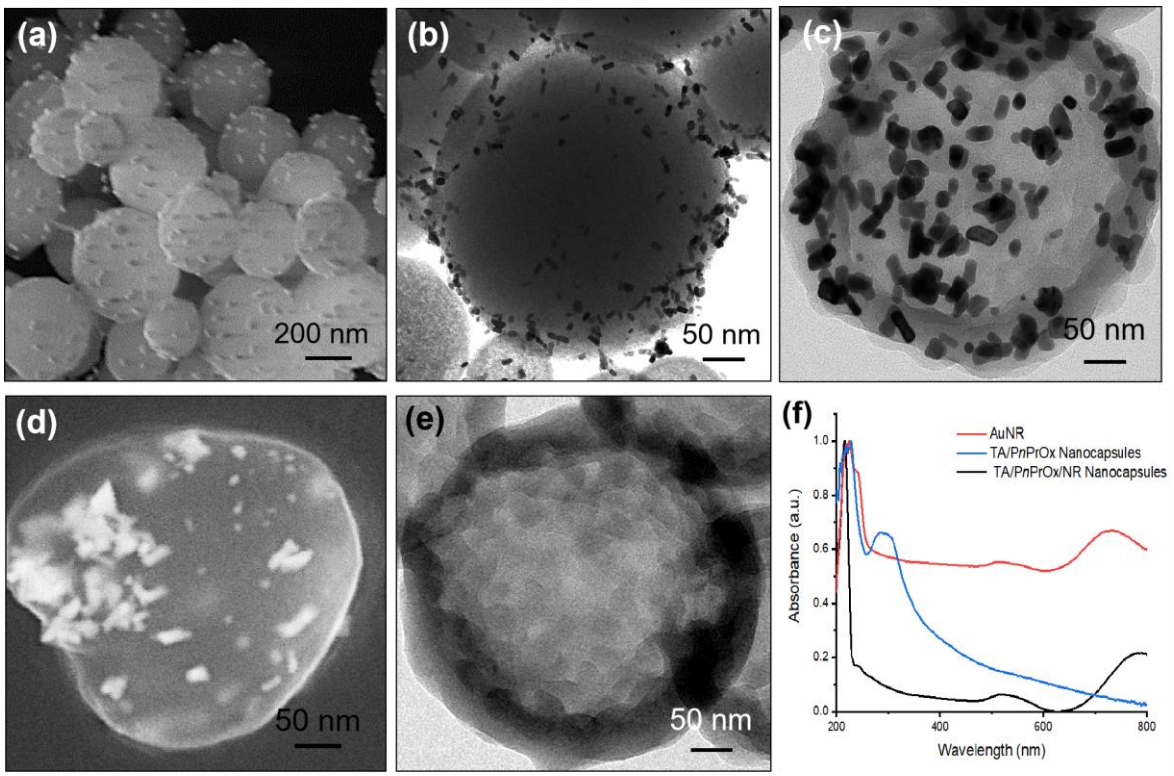

Figure 2. The morphological investigation of *in-situ* modified SiO_2-NR templates and hollow capsules by SEM (a, d) and TEM (b, c and e). The morphology of SiO_2-NR templates (a and b), hollow capsules with preloaded AuNRs (c and d) and control capsules without AuNRs (e). The UV-Visible spectrum of AuNRs, control capsules and modified capsules with AuNRs (f).

The formed capsules were also investigated by UV-Visible spectroscopy prior to and after NR synthesis process (**Figure 2f**). The NRs showed two characteristic peaks at 640 and 800 nm corresponding to the transverse and longitudinal plasmon resonance bands of the gold NRs. The spectrum of control P*n*PrOx/TA nanocapsules showed characteristic peaks corresponding to P*n*PrOx and TA at ~210 and 290 nm, respectively [**24-26**]. However, the capsules showed characteristic peaks of NRs after synthesis process confirming the encapsulation of NRs the interior structure of hollow capsules. In addition, we have also fabricated nanocapsules of PEtOx/TA/NRs and PMeOx/TA/NRs by replacing P*n*PrOx with PEtOx and PMeOx, respectively, to demonstrate the potential of our methodology for other polymer systems within the PAOx family. This also provides a detailed information to check the influence of more hydrophilic entities compared to the thermoresponsive P*n*PrOx. Even though these polymers greatly differ in the aqueous solubility, it did not affect the capsule formation process, as shown in **Figure 3.** The SEM and TEM investigation revealed that the NR encapsulation and distribution was quite similar to that observed in P*n*PrOx capsules. The size of PEtOx/TA/NR and PMeOx/TA/NR nanocapsules was observed to be ~400 nm with a high encapsulation of NRs. Thus, the methodology of *in-situ* NR incorporation in the capsules applies to the other polymeric systems as well, and hence, can be explored for drug delivery and cancer theranostics.

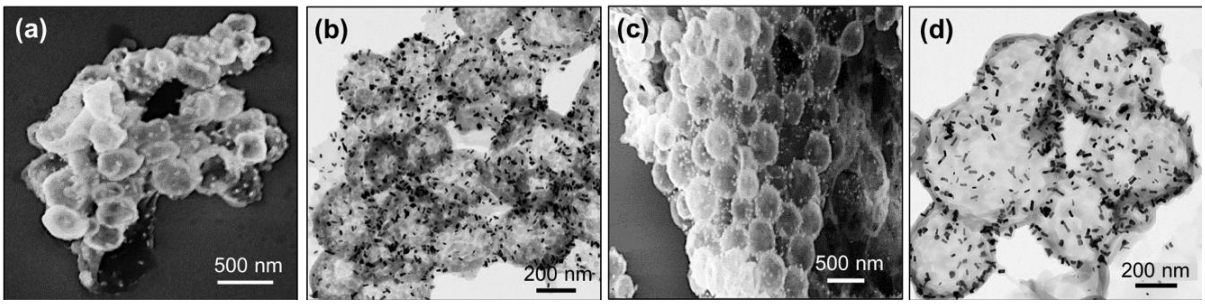

Figure 3. Morphological investigations of (a,b) PMeOx/TA/NR nanocapsules and (c,d) PEtOx/TA/NR nanocapsules by (a,c) SEM and (b,d) TEM.

3.2 Temperature and NIR light-based rupture of nanocapsules

To gain more detailed information about the photo-thermal heat generation and its role in morphological deformation, the P*n*PrOx/TA/NR hollow capsules were exposed to NIR light of 808 nm while the corresponding heat generation was estimated by measuring the increase of temperature. Under laser light exposure, usually NRs absorb light and convert it to heat, thereby increasing the suspension temperature that play a key role in temperature induced

deformation of the hollow capsules. The photothermal heat generation experiments were carried out by adding 0.4 mg of P*n*PrOx/TA/NR capsules in 100 µL of water and exposing them continuously for 5 min with 808 nm solid-state laser, at a power intensity of 0.5 $W.cm^{-2}$ **[20]**. The temperature increase was monitored as a function of time using a probe thermometer and photothermal camera, as shown in **Figure 4a**. The temperature increase was found to be linear in the initial 2-3 min of exposure and almost constant after 3 min. The temperature of the suspension was increased from 28 ºC (room temperature) to 46.6 ºC after 5 min of NIR light exposure. Notably, the PCE was calculated to be 47.5% revealing superior photothermal heat generation under NIR light exposure. After switching off the laser light, the temperature of the nanocapsule suspension cooled down slowly over a period of 10 min as observed under thermal camera imaging **(Supporting Information, Figure S5)**. This process of sudden rise in temperature and slow cooling is considered to be advantageous as it allows enough time for the hyperthermia effect on surrounding cells. Moreover, the P*n*PrOx/TA/NR nanocapsules showed almost 2 to 3 times higher PCE as compared to previously reported structures such as NRs/POMA core-shell structures (18.7%), gold nanoshells (13%), gold vesicles (18%) and $Cu_{2-x}S$ nanocrystals (16.3%) [**12, 27-28**]. A similar experiment was performed with control P*n*PrOx/TA nanocapsules, which showed a negligible temperature rise even after 5 min of NIR irradiation; clearly showing the importance of the NRs for photothermal heat generation.

Further, the morphological investigations of P*n*PrOx/TA/NR nanocapsules under NIR irradiation were explored by SEM and TEM at 27 ºC (**Figure 4b and c**). The capsule morphology changed from a smooth pore-free structure to a porous structure as a function of time. Notably, most of the capsules and their shell ruptured into pieces after NIR radiation of 5 min. Few capsules maintained their shape having surface pores of >100 nm implying temperature induced rupturing of the capsules (**Figure 4b**). The morphological change of the capsule walls is related to the sum of temperature induced rupture of shell in combination with temperature induced dehydration and collapse of P*n*PrOx by configurational reorganization from their hydrated linear form to the collapsed globular form above T_{CP} [**29**]. It was worth noting that this phenomenon was not observed in P*n*PrOx/TA control capsules (**Figure 4d**). In our previous investigations on P*n*PrOx/TA multilayer thin films and microcapsules, the thinning and roughening of the capsules shell followed by rupture was observed at elevated temperatures [**29**]. Subsequently, the capsules were collapsed after 3 h of incubation at 37 ºC. When the same capsules were incubated at 40 ºC, the shell appeared with peaks and valleys on its surface and rupture occurred within 2 h of heat treatment [**5**]. Thus, the increase of capsule

suspension temperature can be effectively used for triggering the release. In this study, the light absorbed by NRs is effectively converted to heat, thereby increasing the suspension temperature which could have played a key role in rupturing the P*n*PrOx/TA shell of the nanocapsules. This demonstrates the ability of the NR-modified capsules to regulate the shell permeability for an on-demand release of the payload. As the biological tissues absorb minimal light in the NIR range, NIR light can be used as a trigger to initiate the release of loaded drug molecules from P*n*PrOx/TA/NR nanocapsules. Hence, these results confirm that P*n*PrOx/TA/NR nanocapsules have potential for use as drug delivery vehicles in cancer therapy.

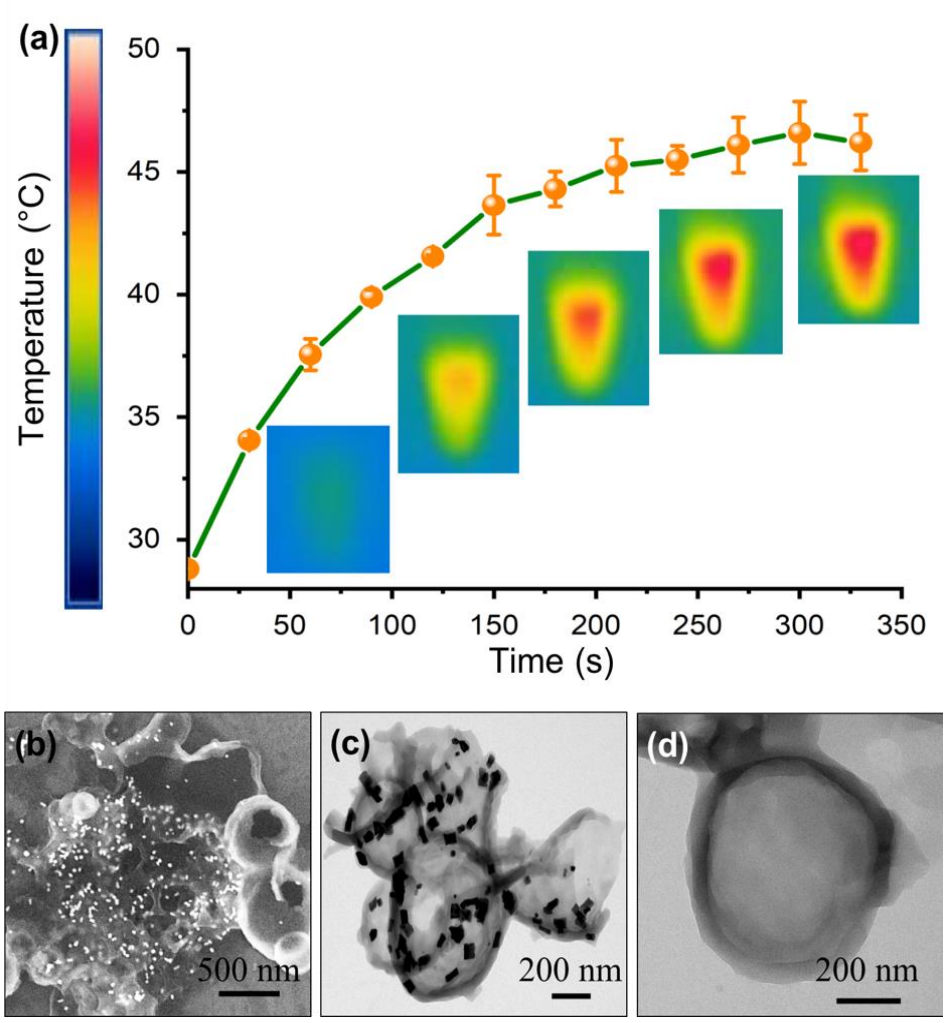

Figure 4. Studies on NIR irradiation of P*n*PrOx/TA/NR nanocapsules using 808 nm, 0.5 W laser. (a) Plot depicting the rise in temperature of capsule suspension along with the images captured by a thermal camera, as a function of time. (b) SEM investigation of NR incorporated capsules after 5 min of laser irradiation. TEM investigation of (c) NR incorporated capsules and (d) control P*n*PrOx/TA nanocapsules after 5 min of laser irradiation.

3.3 Loading and release of DOX at physiological temperature

The P*n*PrOx/TA/NR nanocapsules were then loaded with anticancer drug, DOX by incubating them in drug solution (2 $mg.mL^{-1}$) for 1.5 h. The EE% of DOX was found to be 20%, *i.e.*, 150 μg per mg of dry capsules. The diffusion of DOX from bulk to the interior driven by the concentration gradient is believed to be the major driving for the loading process. Furthermore, the release of the encapsulated DOX from the P*n*PrOx/TA/NR nanocapsules was studied by incubating them in PBS at pH 7.4. A series of samples were kept shaking at 37 ºC and the increase in the supernatant absorbance was assessed as a function of time, using a spectrophotometer. The release of DOX occurred in two different ways: a burst and sustained release at 37 ºC and 16 ºC, respectively, as shown in **Figure 5a and b**. At physiological temperature of 37 ºC, the release was faster initially and slowing down with time. The release was faster initially and slowing down with time. Notably, the %release was calculated to be 55% after 1 h, *i.e.*, 82 μg of DOX. This burst release majorly occurred due to the liberation of surface-bound drug molecules *via* a concentration gradient induced diffusion process. Thereafter, the release was found to be slowing down, and gradually reached a cumulative release of 68% after 2 h of incubation. We believed that the configurational changes from a hydrated linear form to a collapsed globular form at 37 ºC might have also played a key role in enhanced release as it reduces the transport resistance coming from the shell. To gain more detailed information from the diffusion contribution arising from the intact shell wherein P*n*PrOx molecules existing in linear form, the release of DOX was studied at 16 ºC, i.e., at T below the T_{CP} of P*n*PrOx. At this temperature, the capsule shell remains intact and smooth (less porous), thereby leading a release of only 4% even after 2.5 h (**Figure 5b**). To confirm this further, similar encapsulation and release experiments were performed with PEtOx/TA/NR (T_{CP} ~ 60 ºC) and PMeOx/TA/NR (exhibit no LCST behaviour) nanocapsules at 37 ºC (**Supporting information, Figure S6**). Notably, the encapsulation percentages were estimated to be 20 and 16% for PEtOx/TA/NR and PMeOx/TA/NR nanocapsules, respectively matching well with TA/P*n*PrOx/NR nanocapsules below T_{CP}. For both systems, the DOX release was estimated to be < 9% after 2 h which increased to ~14% even after 10 h of release process. It is worth noting that their release profiles were almost the same as TA/P*n*PrOx/NR nanocapsules at 16 ºC. Hence, it can be concluded that the in-built temperature responsiveness of the P*n*PrOx capsules at a temperature above the T_{CP} of P*n*PrOx helps in triggering the release of encapsulated DOX in a burst manner in physiological conditions (37 ºC).

The release of DOX from the P*n*PrOx/TA/NR nanocapsules was also studied under the exposure of 808 nm NIR laser for up to 30 min. As NRs exhibited a high absorbance in the range of 780 nm to 810 nm (**Figure 2f**), a standard solid-state laser of 808 nm was selected for the investigation of NIR light induced release process. The NRs tend to absorb light and produce heat, thereby increasing the local temperature. Due to a sudden rise in temperature of up to 46 ºC (refer photothermal heat generation section), the polymeric shell of P*n*PrOx/TA nanocapsules gets ruptured quickly that leads to enhanced release of DOX. Notably, a burst release of ~56.5% of the DOX was observed within 2 min, and it reached a maximum of 72% cumulative release within 30 min of exposure (**Figure 5a and b**). The NIR light induced release is highly advantageous for cancer therapy as it increases the local concentration quickly in the tumor environment while maintaining the cancer cells at T > 46 ºC by photothermal heat generation. As a result, the combination of chemotherapy and hyperthermia might inflict major damage to cancer cells and improve the apoptosis process. Thus, the modified P*n*PrOx/TA nanocapsules will help us to achieve an on-demand release of payload in the form of combined burst and sustained release for cancer theranostic applications.

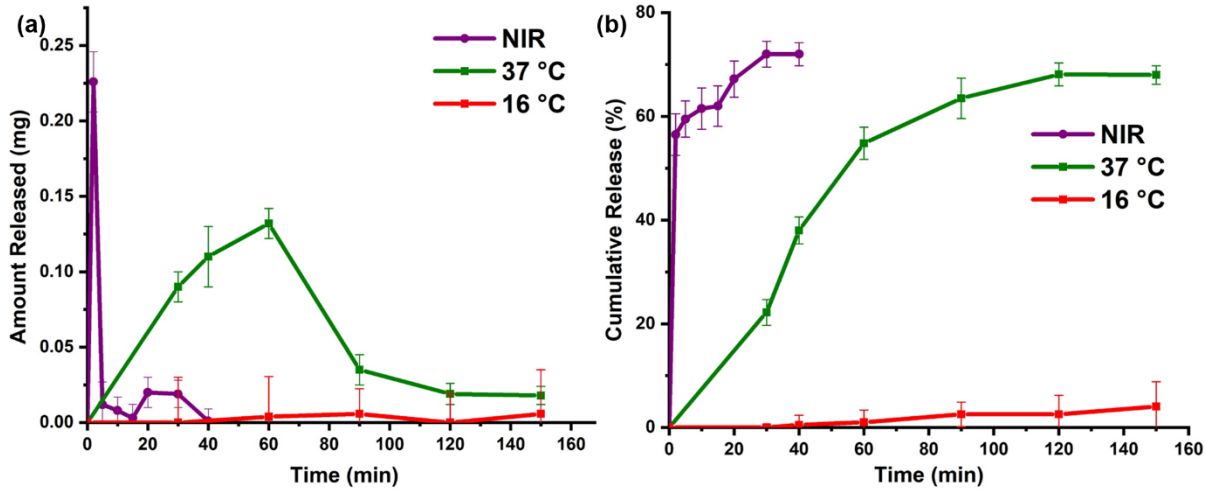

Figure 5. (a) The amount released and (b) cumulative %release of DOX from the P*n*PrOx/TA/NR nanocapsules at 37 ºC, 16 ºC and under NIR irradiation at 37 ºC.

3.4 Anticancer activity

The cytotoxic activity of the nanocapsules was studied against HEp-2 epithelial cell line derived from larynx carcinoma to demonstrate their potential in cancer therapy. Prior to anticancer activity investigations, the cells were treated with free DOX of varying concentration to identify the IC_{50} value of DOX towards HEp-2 cells. The percentage of live and dead cell populations were estimated by alamar blue assay. The IC_{50} value was estimated

to be ~15 µM. Based on this value, the further use of DOX in free form and encapsulated form during the cell experiments was maintained at ~5 µM for all samples. The dilutions of Cap-DOX were made in such a way that it contains ~5 µM of drug, and this amount was added to wells during the experiment. In our previous study, we have demonstrated that even well below IC_{50} value, the cancer cells undergo apoptosis when the local drug concentration was increased above IC_{50} value [**30**]. Hence, we maintained the drug concentration lower than IC_{50} value for the whole experiments. To investigate the cytotoxicity of P*n*PrOx/TA/NR capsules, different samples were analysed for cytotoxicity measurement including cells treated with only NIR light, P*n*PrOx/TA/NR capsules (Cap), P*n*PrOx/TA/NR-DOX capsules (Cap-DOX), P*n*PrOx/TA/NR capsules exposed to NIR light (Cap-NIR light) and P*n*PrOx/TA/NR-DOX capsules exposed to NIR light (Cap-DOX-NIR). The control cells treated with only NIR light were observed to maintain their viability of ~90% even after 5 min of laser light irradiation and incubation of 24 h in the medium indicating the absence of cytotoxic effect (**Figure 6a**). Similar results were obtained when the HEp-2 cells were treated with only NRs or P*n*PrOx/TA/NR nanocapsules for 24 h, showing 92 and 93% of cell viability, respectively. When the cells were treated with pure DOX (~5 µM) and DOX loaded P*n*PrOx/TA/NR nanocapsules containing ~5 µM of drug, the cell viability was decreased to ~70% and ~63%, respectively, due to the induced chemotherapeutic effect. Notably, the availability of only 68% of drug from the nanocapsules led to the decreased viability of the cells. Similarly, when the cells incubated with P*n*PrOx/TA/NR nanocapsules were irradiated with NIR light for 5 min, the viability decreased to 73%, most likely due to the hyperthermia effect caused by photothermal heat generation. In other words, a sudden rise in the local temperature caused by photothermal heat generation of NRs leads to a significant PTT effect, thereby inducing cancer cell apoptosis. Interestingly, when the cells were treated with DOX loaded P*n*PrOx/TA/NR nanocapsules along with 5 min NIR irradiation, a synergistic effect of both chemotherapy and PTT led to a significant rise in cell death leaving only about 10% viable cells. Importantly, the instant pulse release of DOX within few minutes of exposure causes an increase in the local concentration of the drug way beyond its IC_{50} [**30**]. Hence, it shoots up apoptosis in much higher number of cells and inducing enhanced cell death.

The suspension of apoptotic PI stained HEp-2 cells was collected after treatment with P*n*PrOx/TA/NR nanocapsules along with DOX and NIR irradiation and was investigated under confocal laser scanning microscopy (CLSM), as shown in **Figure 6b and c**. It was observed that groups of nanocapsules were mostly gathered and clinged to the cell membrane. This was since the cells can adhere and grow more easily on hydrophobic surfaces than on hydrophilic

surfaces because of the difficulty of displacing adsorbed water molecules in the latter [**31, 32**]. As a result, when the cells are treated with capsules along with NIR irradiation, the suspension temperature rises above the T_{CP} and P*n*PrOx tends to behave as hydrophobic surface, causing the adhesion of capsules to the cells. As DOX is released near the cancer cells, it increases the local concentration of drug way beyond its IC_{50} leading to apoptosis [**30**]. Further, it has been previously reported that amphiphilic PAOx efficiently enters cells *via* endocytosis and their hydrophobicity plays an important role in the uptake of these polymers [**33-35**]. Although the cellular internalization was not studied in this work, the arrows marked in **Figure 6b** shows the possibility of cellular internalization of the nanocapsules. In general, PAOx appears to be well tolerated by mammalian cells. Raveendran *et al.* reported the successful cellular internalization of PAOx NPs loaded with curcumin [**36**]. The uptake of various diblock and triblock copolymers have been successfully reported in MCF7-ADR cells, MCF7 cells, cartilage discs, dermal fibroblasts and human endothelial cells [**37-40**].

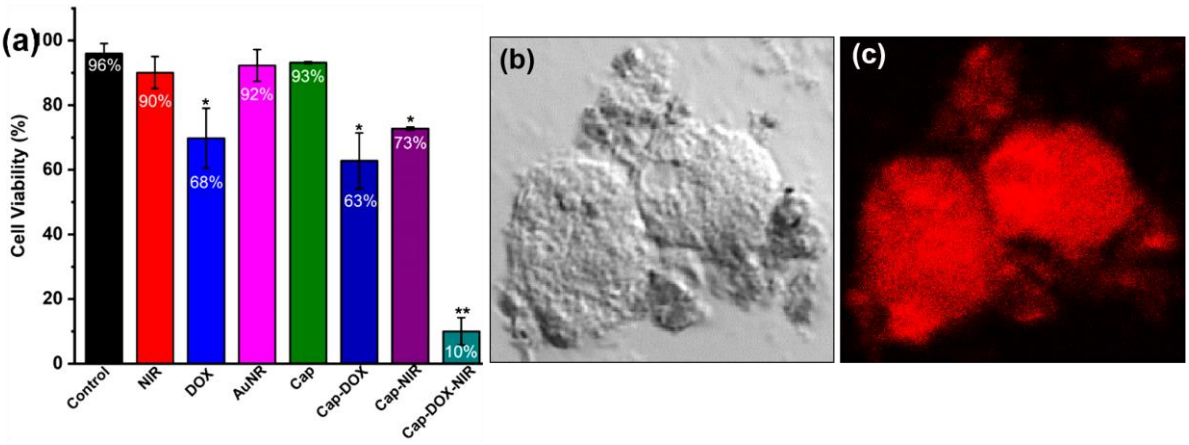

Figure 6. (a) Cell viability studies of HEp-2 cancer cells after treatment with 808 nm NIR light, DOX, NRs, P*n*PrOx/TA/NR nanocapsules, capsules encapsulated with DOX, capsules along with NIR exposure, and lastly capsules encapsulated with DOX and NIR exposure. CLSM image of PI-stained apoptotic cells surrounded by groups of nanocapsules (denoted by arrows) as imaged in (b) bright field and (c) red channel.

To gain further knowledge on the change in morphology of the HEp-2 cancer cells, they were treated with similar samples and stained with AO and PI fluorescent dyes, to image the live and dead cell population (**Figure 7**). AO tends to permeate both the live and dead cells by intercalating with DNA and RNA, thus, staining both the live and dead populations and

make them appear in green color. On the other hand, PI tags only the apoptotic cells whose membrane has been compromised in red color. For the control samples, all the cells appeared in green colour with a negligible amount of PI staining, as shown in **Figure 7a-d**. Similar results were obtained when the cells were treated with 808 nm NIR laser irradiation, NRs and P*n*PrOx/TA/NR nanocapsules, showing high cell viability ranging from 90-93% as shown in **Figure 7e-p**. An almost insignificant number of cells showed uptake of PI, suggesting that the NIR radiation, NRs and the P*n*PrOx/TA polymers do not display any cytotoxic effect on the cancer cells. On the other hand, when the cells were treated with P*n*PrOx/TA/NR capsules followed by NIR irradiation, the PI uptake in the cells increased indicating the increased number of cell death, most likely caused by the PTT effect (**Figure 7q-t**). The number of PI stained cells further increased when they were treated with DOX encapsulated capsules (**Figure 7u-x)**. Lastly, a maximum number of cells were stained with PI when they were treated with DOX encapsulated capsules followed by NIR irradiation, due to the synergistic effect of PTT and chemotherapy (**Figure 7y-zb**). The NIR radiation not only resulted in elevated local temperature but also induced burst release of DOX that might have increased local concentration much higher than the IC_{50} value. The combined chemo-photo-therapeutic effect probably resulted in apoptosis followed by death of a greater number of cells. The orange color in the superimposed images denotes the actual apoptotic population of cells. The object count of red and green objects in each image was also analyzed by the software and the cell viability percentages matched to the one's obtained from the alamar blue assay (**Supporting Information, Table T3)**. Moreover, the apoptosis of cells treated with DOX encapsulated capsules and NIR as a function of time is shown in **Figure 8**. Notably, the effect of dual chemo-photothermal treatment started within a couple of hours leaving majority of cell to undergo apoptosis visibly within first 6 h (**Figure 8b-d**). The simultaneous spike in local DOX concentration and temperature in tumor environment probably led to unfavourable conditions for the cancer cells and resulted in spherical cells, rupturing of cell membrane and cell death. Hence, these results suggest that the proposed nanocapsules may prove to be an effective and quick treatment therapy for *in-vitro* and *in-vivo* applications.

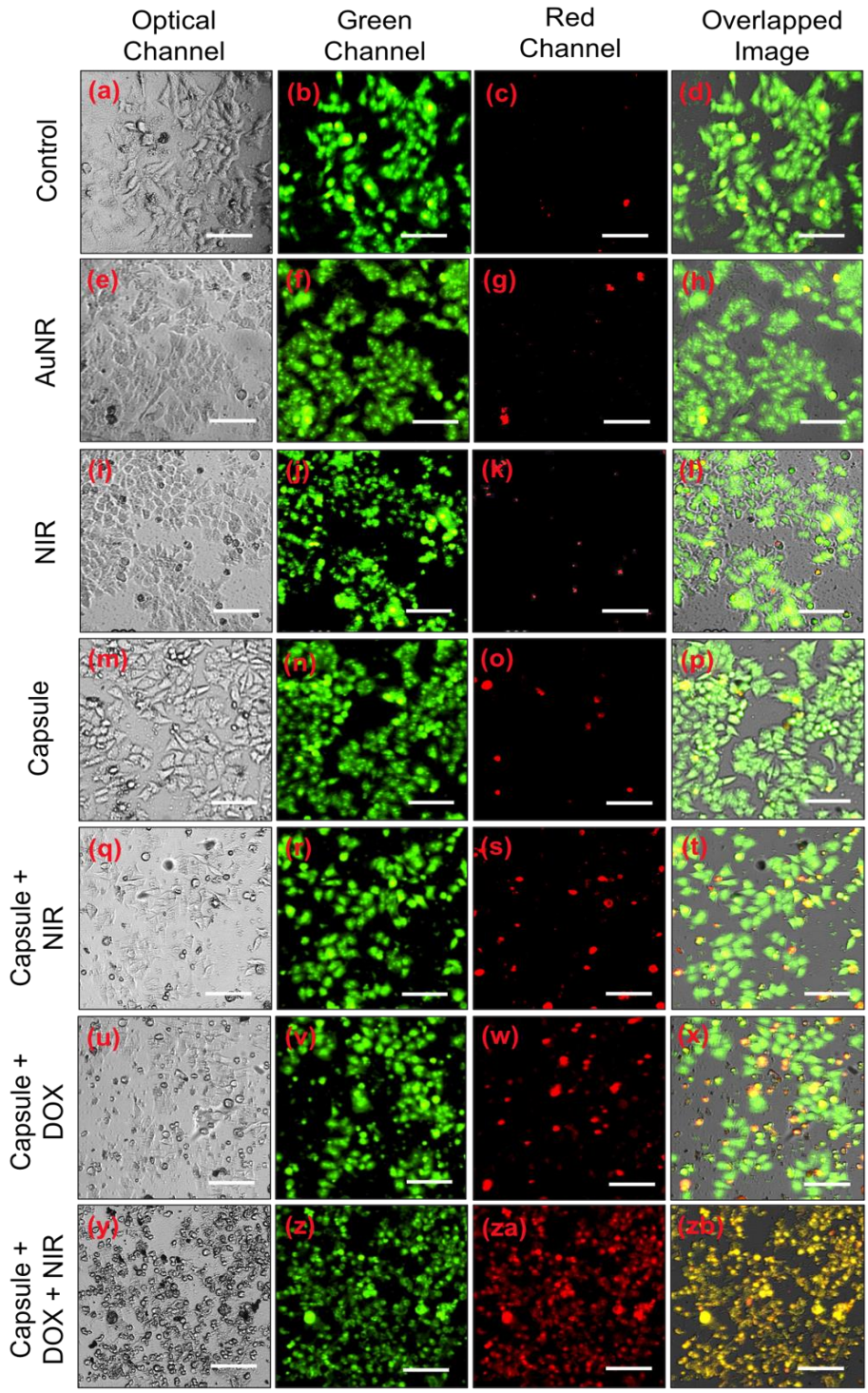

Figure 7. Anticancer experiments showing the live and apoptotic cell populations. Control cells (a-d) and cells treated with (e-h) NRs, (i-l) NIR, (m-p) P*n*PrOx/TA/NR capsules, (q-t) P*n*PrOx/TA/NR capsules irradiated with NIR, (u-x) DOX incorporated P*n*PrOx/TA/NR capsules, (y-zb) DOX incorporated P*n*PrOx/TA/NR capsules followed by their NIR exposure. The cells were stained with AO and PI to visualize them in green (live cells) and red colour (apoptotic/dead cells), respectively. The scale bar denotes 100 µm.

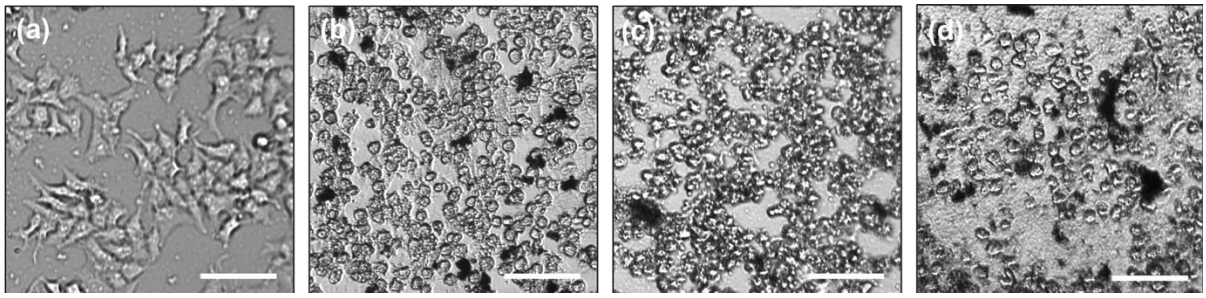

Figure 8. Anticancer activity investigations showing progress in cell death at (a) 0 h, (b) 6 h, (c) 15 h and (d) 24 h after treatment with DOX incorporated P*n*PrOx/TA/NR nanocapsules followed by their NIR exposure. The scale bar denotes 100 µm.

The wide applicability of the proposed method was also confirmed by conducting similar cell cytotoxicity experiments against other cell lines. The P*n*PrOx/TA/NR nanocapsules and dual-therapeutic effect of PTT and chemotherapy proved equally effective on HT1080 fibrosarcoma cells, as shown in **Figure 9 and 10**. The IC_{50} value of DOX towards HT-1080 cells was determined to be ~ 4 µM. To investigate the cytotoxicity of P*n*PrOx/TA/NR capsules against HT-1080 cells, similar experiments were designed as discussed in the previous section. The control cells, cells treated with 5 min of NIR light exposure, cells treated with only NRs and cells treated with only capsules were observed to maintain their viability at ~97, 96, 93 and 93%, respectively after 24 h of incubation in the medium indicating no significant cytotoxic effect (**Figure 9**). Similarly, when the cells were treated with a solution of pure DOX of similar concentration, the viability decreased to 75%. However, when the cells were treated with DOX loaded capsules (~ 4 µM), the viability reduced to 50% due to the availability of only 68% of encapsulated drug, as explained in section 3.3. Further, upon treatment with DOX loaded capsules along with 5 min of NIR exposure, a synergistic effect of chemotherapy and PTT led to a significant decrease in the cell viability leaving only 19% viable cells.

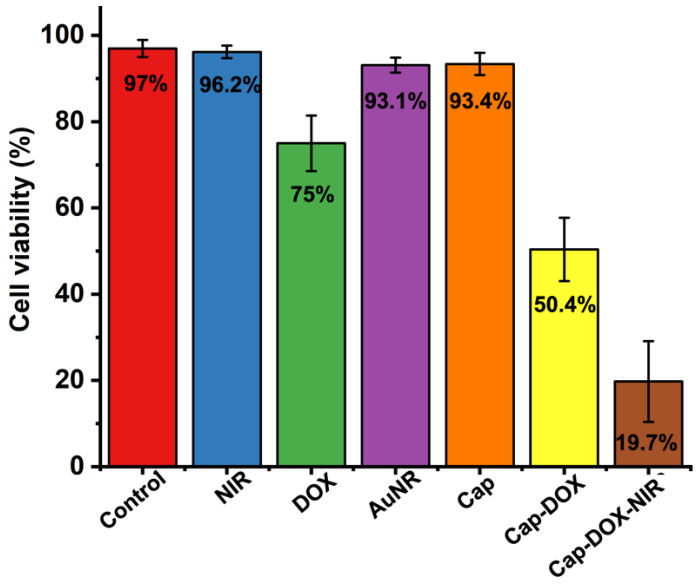

Figure 9. Cell viability studies of HT1080 cancer cells after treatment with 808 nm NIR light, DOX, gold NRs, P*n*PrOx/TA/NR nanocapsules, capsules encapsulated with DOX, and lastly capsules along with both DOX encapsulation and NIR exposure.

The change in morphology of the cancer cells was investigated by treating the HT1080 cells with similar samples followed by their staining with AO and EtBr fluorescent dyes to image the live and dead cell population (**Figure 10**). Like with PI, EtBr also tags only the apoptotic cells whose membrane has been compromised (red colour). Thus for the control cells, all the cells appear green with a negligible number of EtBr stained cells, as shown in **Figure 10a-d**. Similar results were obtained when the cells were treated with only NIR irradiation and only P*n*PrOx/TA/NR capsules as shown in **Figure 10e-l**. Almost insignificant amount of cells show uptake of EtBr, suggesting that the NIR radiation and the P*n*PrOx/TA nanocapsules do not display any cytotoxicity to the cells. On the other hand, when the capsules were encapsulated with DOX, the cell viability decreased accounting for the chemotherapeutic effect (**Figure 10m-p**). Interestingly, the viability reached ~19% when the cells were treated with both DOX incorporated capsules along with NIR irradiation as most of the cells were stained by EtBr, accounting to the synergistic chemotherapy and PTT effect (**Figure 10q-t**). The superimposed images showed an appearance of orange colour, which denoted the actual apoptotic population. The results suggest the effective use of P*n*PrOx/TA/NR capsules for *in-vitro* and *in-vivo* applications.

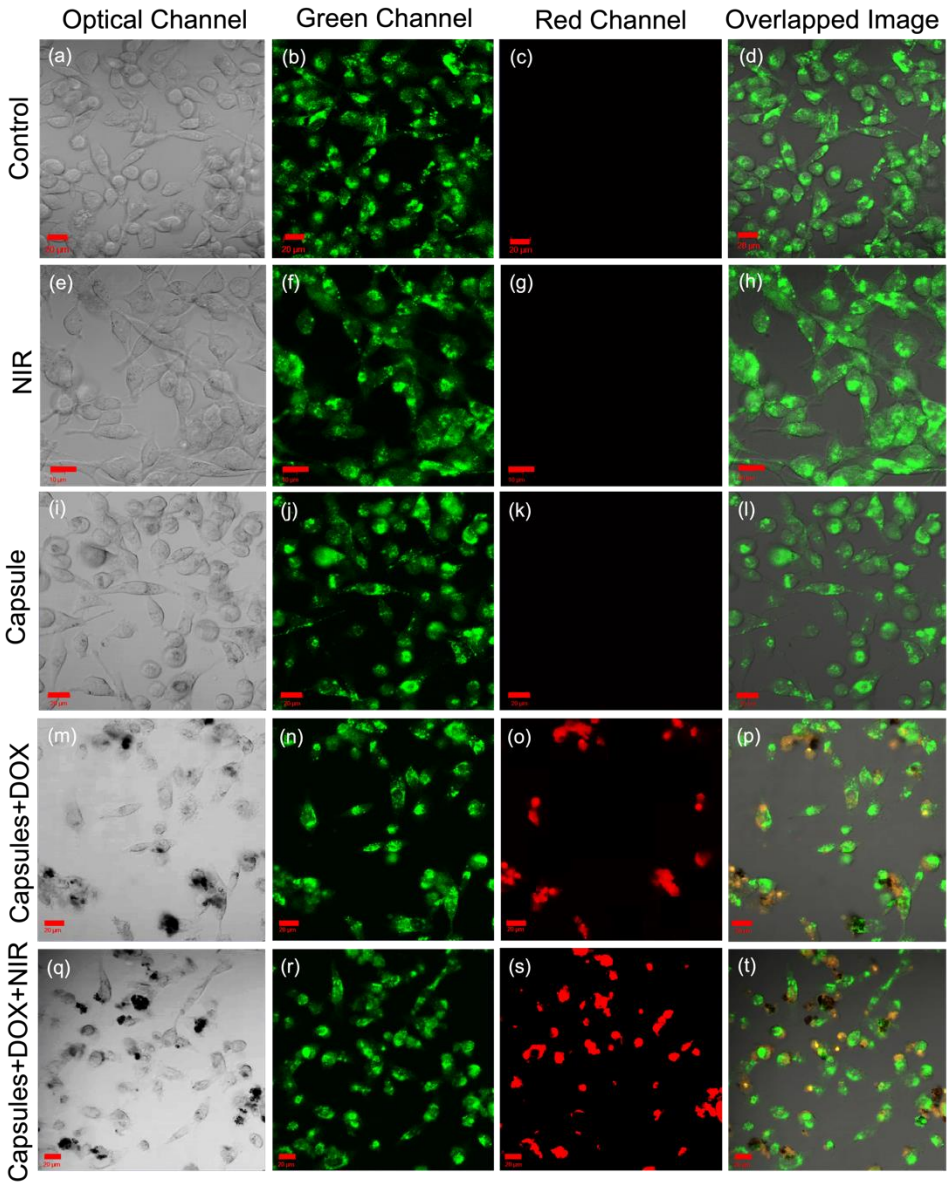

Figure 10. Anticancer experiments showing the live and apoptotic cell population of HT1080 cells. Control cells (a-d) and cells treated with NIR (e-h), P*n*PrOx/TA/NR capsules (i-l), DOX incorporated P*n*PrOx/TA/NR capsules (m-p), DOX incorporated P*n*PrOx/TA/NR capsules followed by their NIR exposure (q-t). The cells were stained with AO and EtBr to visualize them in green (live cells) and red (apoptotic/dead cells) color, respectively. The scale bar denotes 20 µm.

4. CONCLUSIONS

We have reported hydrogen bonded LBL formation of temperature responsive P*n*PrOx/TA nanocapsules for cancer chemo-photothermal therapy. A new methodology has been reported to *in-situ* synthesize gold NRs in the interior structure of mesoporous silica NPs which is later used as sacrificial template for LbL assembly. The LbL assembly of TA and

P*n*PrOx on NR containing silica NPs followed by core dissolution resulted in hollow P*n*PrOx/TA nanocapsules preloaded with uniformly distributed NRs. Under NIR light exposure at 808 nm and 0.5 $W.cm^{-2}$, the temperature of capsules suspension was increased up to 47 ºC owing to photothermal heat generation of incorporated NRs. The amount of DOX loading was estimated to be 150 μg per mg of nanocapsules. While the diffusion-controlled process showed sustained release up to 10 h at 16 ºC, the NIR exposure resulted in burst release of DOX at 37 ºC within 5 min, thus, paving the way for using this system as sustained and `on-demand burst release` drug delivery carriers. In anti-cancer activity experiments, the increase of suspension temperature after NIR exposure might have increased hydrophobicity of capsules which in turn improved cellular uptake of drug loaded capsules by cancer cells via hydrophobic interactions. As a result, the reported capsules showed excellent anticancer activity against HEp-2 epithelial cells (~90% cell death) and HT1080 fibrosarcoma cells (~81% cell death). Notably, the photo-thermal heat generation of NRs not only resulted in enhanced drug release from the capsules but also induced hyperthermia by elevating the local temperature in the tumor environment, *i.e.,* chemo-photo-thermal therapy. The *in-situ* synthesis methodology was successfully performed in other PAOx systems as well to demonstrate their potential for wider applicability. Hence, the proposed nanocapsules have future potential for combined chemo-PTT therapy for cancer treatment.

ACKNOWLEDGEMENTS

Dr. Anandhakumar S. acknowledges financial support from the Department of Science and Technology (DST) - Science and Engineering Research Board (SERB) (File No. CRG/2020/004175) and Council of Scientific and Industrial Research (CSIR) (Application no. 09/1045/0036 2K19 EMR-1), Government of India. The authors acknowledge SRM Institute of Science and Technology for providing research facilities. Prof. Richard Hoogenboom thanks Ghent University and FWO for continuous financial support of the research.

CONFLICT OF INTEREST

The authors declare no competing financial interest.

REFERENCES

[1] L. Tauhardt, K. Kempe, M. Gottschaldt, U.S. Schubert, Poly (2-oxazoline) functionalized surfaces: from modification to application, Chem. Soc. Rev. *42*(20) (2013) 7998-8011. https://doi.org/10.1039/C3CS60161G.

[2] K. Kempe, S.L. Ng, K.F. Noi, M. Müllner, S.T. Gunawan, F. Caruso, Clickable poly (2-oxazoline) architectures for the fabrication of low-fouling polymer capsules, ACS Macro Lett. *2*(12) (2013) 1069-1072. https://doi.org/10.1021/mz400522e.

[3] R. Konradi, C. Acikgoz, M. Textor, Polyoxazolines for nonfouling surface coatings—a direct comparison to the gold standard PEG, Macromol. Rapid Commun. *33*(19) (2012) 1663-1676. https://doi.org/10.1002/marc.201200422.

[4] F.C. Gaertner, R. Luxenhofer, B. Blechert, R. Jordan, M. Essler, Synthesis, biodistribution and excretion of radiolabeled poly (2-alkyl-2-oxazoline)s, J. Control. Release. *119*(3) (2007) 291-300. https://doi.org/10.1016/j.jconrel.2007.02.015.

[5] N. Mathivanan, G. Paramasivam, M. Vergaelen, J. Rajendran, R. Hoogenboom, A. Sundaramurthy, Hydrogen-bonded multilayer thin films and capsules based on poly (2-n-propyl-2-oxazoline) and tannic acid: investigation on intermolecular forces, stability, and permeability, Langmuir. *35*(45) (2019) 14712-14724. https://doi.org/10.1021/acs.langmuir.9b02938.

[6] V. Sharma, G. Paramasivam, M. Vergaelen, R. Hoogenboom, A. Sundaramurthy, Tannic Acid-Stabilized Self-Degrading Temperature-Sensitive Poly (2-n-propyl-2-oxazoline)/Gellan Gum Capsules for Lipase Delivery. ACS Appl. Bio Mater. *4*(9) (2021) 7134-7146. https://doi.org/10.1021/acsabm.1c00697.

[7] F. Wang, P. Ren, K.V. Bernaerts, Y. Fu, W. Hu, N. Zhou, T. Zhang, Thermoresponsive Poly (2-propyl-2-oxazoline) Surfaces of Glass for Nonenzymatic Cell Harvesting, ACS Appl. Bio Mater. *3*(8) (2020) 5428-5437. https://doi.org/10.1021/acsabm.0c00650.

[8] M. Kuepfert, E. Ahmed, M. Weck, Self-Assembled Thermoresponsive Molecular Brushes as Nanoreactors for Asymmetric Aldol Addition in Water, Macromol. 54(8) (2021) 3845-3853. https://doi.org/10.1021/acs.macromol.0c02708.

[9] V. Sharma, A. Sundaramurthy, Reusable hollow polymer microreactors incorporated with anisotropic nanoparticles for catalysis application, ACS Omega. *4*(1) (2019) 628-636. https://doi.org/10.1021/acsomega.8b02820.

[10] V. Sharma, J. Vijay, M.R. Ganesh, A. Sundaramurthy, Multilayer capsules encapsulating nimbin and doxorubicin for cancer chemo-photothermal therapy, Int. J. Pharm. 582 (2020) 119350. https://doi.org/10.1016/j.ijpharm.2020.119350.

[11] H.Y. Koo, W.S. Choi, D.Y. Kim, Direct growth of optically stable gold nanorods onto polyelectrolyte multilayered capsules, Small. *4*(6) (2008) 742-745. https://doi.org/10.1002/smll.200800021.

[12] S. Vial, I. Pastoriza-Santos, J. Pérez-Juste, L.M. Liz-Marzán, Plasmon coupling in layer-by-layer assembled gold nanorod films, Langmuir. *23*(8) (2007) 4606-4611. https://doi.org/10.1021/la063753t.

[13] J. Wang, C. Zhu, J. Han, N. Han, J. Xi, L. Fan, R. Guo, Controllable synthesis of gold nanorod/conducting polymer core/shell hybrids toward in vitro and in vivo near-infrared photothermal therapy, ACS Appl. Mater. Interfaces. *10*(15) (2018) 12323-12330. https://doi.org/10.1021/acsami.7b16784.

[14] X. Chen, Q. Zhang, J. Li, M. Yang, N. Zhao, F.J. Xu, Rattle-structured rough nanocapsules with in-situ-formed gold nanorod cores for complementary gene/chemo/photothermal therapy, ACS Nano. *12*(6) (2018) 5646-5656. https://doi.org/10.1021/acsnano.8b01440.

[15] E.F.J. Rettler, M.V. Unger, R. Hoogenboom, H.W. Siesler, U.S. Schubert, Water uptake of poly (2-N-alkyl-2-oxazoline)s: temperature-dependent Fourier transform infrared (FT-IR) spectroscopy and two-dimensional correlation analysis (2DCOS), Appl. Spectrosc. *66*(10) (2012) 1145-1155. https://doi.org/10.1366/12-06650.

[16] A. Sundaramurthy, V. Nagaraja, A.M. Raichur, Reversible polyelectrolyte capsules as carriers for protein delivery, Colloids Surf. B. *78*(2) (2010) 266-274. https://doi.org/10.1016/j.colsurfb.2010.03.016.

[17] A. Sundaramurthy, M. Debapriya, V. Nagaraja, A.M. Raichur, Polyelectrolyte microcapsules for sustained delivery of water-soluble drugs, Mater. Sci. Engg. C. 31(2) (2011) 342-349. https://doi.org/10.1016/j.msec.2010.10.005.

[18] V. Sharma, A. Sundaramurthy, M. Sasidharan, Self-degrading niosomes for encapsulation of hydrophilic and hydrophobic drugs: an efficient carrier for cancer multi-drug delivery, Mater. Sci. Engg. C. 56 (2015) 393-400.

[19] N. Samed, V. Sharma, A. Sundaramurthy, Hydrogen bonded niosomes for encapsulation and release of hydrophilic and hydrophobic anti-diabetic drugs: an efficient system for oral anti-diabetic formulation, Appl. Surf. Sci. 449 (2018) 567-573. https://doi.org/10.1016/j.apsusc.2017.11.055.

[20] A. Sundaramurthy, S.P. Vijayalakshmi, G. Jagadeesh, A.M. Raichur, Silver nanoparticle synthesis: novel route for laser triggering of polyelectrolyte capsules. ACS Appl. Mater. Interfaces. *3*(9) (2011) 3419-3424. https://doi.org/10.1021/am200651t.

[21] A. Sundaramurthy, A.M. Raichur, A facile route to synthesize silver nanoparticles in polyelectrolyte capsules, Colloids Surf. B. *84*(2) (2011) 379-383. https://doi.org/10.1016/j.colsurfb.2011.01.029.

[22] A. Sundaramurthy, V. Mahalakshmi, A.M. Raichur, Silver nanoparticles modified nanocapsules for ultrasonically activated drug delivery, Mater. Sci. Engg. C. 32(8) (2012) 2349-2355. https://doi.org/10.1016/j.msec.2012.07.006.

[23] V. Sharma, A. Sundaramurthy, Surface modification of bare copper grids with charged polymers: A simple alternative for carbon coated copper grids in transmission electron microscopy, Mater. Lett. 308 (2022) 131204. https://doi.org/10.1016/j.matlet.2021.131204.

[24] R. Hoogenboom, M.W. Fijten, H.M. Thijs, B.M. van Lankvelt, U.S. Schubert, Microwave-assisted synthesis and properties of a series of poly (2-alkyl-2-oxazoline)s, Des. Monomers Polym. 8(6) (2005) 659-671. https://doi.org/10.1163/156855505774597704.

[25] R. Hoogenboom, Poly (2-oxazoline)s: a polymer class with numerous potential applications, Angew. Chem. Int. Ed. 48(43) (2009) 7978-7994. https://doi.org/10.1002/anie.200901607.

[26] A. Sundaramurthy, M. Vergaelen, S. Maji, R. Auzély-Velty, Z. Zhang, B.G. De Geest, R. Hoogenboom, Hydrogen Bonded Multilayer Films Based on Poly (2-oxazoline) s and Tannic

Acid, Adv. Healthc. Mater. 3(12) (2014) 2040-2047. https://doi.org/10.1002/adhm.201400377.

[27] P. Huang, J. Lin, W. Li, P. Rong, Z. Wang, S. Wang, X. Wang, X. Sun, M. Aronova, G. Niu, R.D. Leapman, Z. Nie, X. Chen, Biodegradable Gold Nanovesicles with an Ultrastrong Plasmonic Coupling Effect for Photoacoustic Imaging and Photothermal Therapy, Angew. Chem. Int. Ed. 52 (2013) 13958-13964. https://doi.org/10.1002/ange.201308986.

[28] S. Wang, A. Riedinger, H. Li, C. Fu, H. Liu, L. Li, T. Liu, L. Tan, M.J. Barthel, G. Pugliese, Plasmonic Copper Sulfide Nanocrystals Exhibiting Near Infrared Photothermal and Photodynamic Therapeutic Effects, ACS Nano. 9 (2015) 1788-1800. https://doi.org/10.1021/nn506687t.

[29] G. Paramasivam, M. Vergaelen, M.R. Ganesh, R. Hoogenboom, A. Sundaramurthy, Hydrogen bonded capsules by layer-by-layer assembly of tannic acid and poly (2-n-propyl-2-oxazoline) for encapsulation and release of macromolecules, J. Mater. Chem. B. 5(45) (2017) 8967-8974. https://doi.org/10.1039/C7TB02284K.

[30] B. Bhargawa, V. Sharma, M.R. Ganesh, F. Cavalieri, M. Ashokkumar, B. Neppolian, B., A. Sundaramurthy, Lysozyme microspheres incorporated with anisotropic gold nanorods for ultrasound activated drug delivery, Ultrason. Sonochem. 86 (2022) 106016. https://doi.org/10.1016/j.ultsonch.2022.106016.

[31] N. Yamada, T. Okano, H. Sakai, F. Karikusa, Y. Sawasaki, Y. Sakurai, Thermo-responsive polymeric surfaces; control of attachment and detachment of cultured cells, Die Makromolekulare Chemie, Rapid Commun. 11(11) (1990) 571-576. https://doi.org/10.1002/marc.1990.030111109.

[32] A. Dworak, A. Utrata-Wesołek, N. Oleszko, W. Wałach, B. Trzebicka, J. Anioł, A.L. Sieroń, A. Klama-Baryła, M. Kawecki, Poly (2-substituted-2-oxazoline) surfaces for dermal fibroblasts adhesion and detachment, J. Mater. Sci.: Mater. Med. 25(4) (2014) 1149-1163. https://doi.org/10.1007/s10856-013-5135-7.

[33] N. Zhang, T. Pompe, I. Amin, R. Luxenhofer, C. Werner, R. Jordan, Tailored poly (2-oxazoline) polymer brushes to control protein adsorption and cell adhesion, Macromol. Biosci. 12(7) (2012) 926-936. https://doi.org/10.1002/mabi.201200026.

[34] J. Tong, R. Luxenhofer, X. Yi, R. Jordan, A.V. Kabanov, Protein modification with amphiphilic block copoly (2-oxazoline)s as a new platform for enhanced cellular delivery, Mol. Pharmaceutics. *7*(4) (2010) 984-992. https://doi.org/10.1021/mp100102p.

[35] V.R. de la Rosa, Poly (2-oxazoline)s as materials for biomedical applications, J. Mater. Sci.: Mater. Med. 25(5) (2014) 1211-1225. https://doi.org/10.1007/s10856-013-5034-y.

[36] R. Raveendran, K.M. Mullen, R.M. Wellard, C.P. Sharma, R. Hoogenboom, T.R. Dargaville, Poly (2-oxazoline) block copolymer nanoparticles for curcumin loading and delivery to cancer cells, Eur. Polym. J. 93 (2017) 682-694. https://doi.org/10.1016/j.eurpolymj.2017.02.043.

[37] M. Barz, R. Luxenhofer, R. Zentel, A.V. Kabanov, The uptake of N-(2-hydroxypropyl)-methacrylamide based homo, random and block copolymers by human multi-drug resistant

breast adenocarcinoma cells, Biomater. 30(29) (2009) 5682-5690. https://doi.org/10.1016/j.biomaterials.2009.06.058.

[38] R. Luxenhofer, G. Sahay, A. Schulz, D. Alakhova, T.K. Bronich, R. Jordan, A.V. Kabanov, Structure-property relationship in cytotoxicity and cell uptake of poly (2-oxazoline) amphiphiles, J. Control. Release. 153(1) (2011) 73-82. https://doi.org/10.1016/j.jconrel.2011.04.010.

[39] O. Berberich, J. Blöhbaum, S. Hölscher-Doht, R.H. Meffert, J. Teßmar, T. Blunk, J. Groll, Catechol-modified poly (oxazoline) s with tunable degradability facilitate cell invasion and lateral cartilage integration, J. Ind. Eng. Chem. 80 (2019) 757-769. https://doi.org/10.1016/j.jiec.2019.06.038.

[40] B.J. Chang, O. Prucker, E. Groh, A. Wallrath, M. Dahm, J. Rühe, Surface-attached polymer monolayers for the control of endothelial cell adhesion, Colloids Surf. A: Physicochem. Eng. 198 (2002) 519-526. https://doi.org/10.1016/S0927-7757(01)00952-9.